Paleoceanography and Paleoclimatology

RESEARCH ARTICLE
10.1029/2019PA003789

Persistent East Equatorial Pacific Carbon Storage at the Middle Pleistocene Transition

Paula Diz[1], Antonio Cobelo-García[2], Iván Hernández-Almeida[3], Hugo Corbí[4], and Stefano M. Bernasconi[3]

[1]Departamento de Geociencias Marinas, Universidade de Vigo, Vigo, Spain, [2]Instituto de Investigaciones Marinas, CSIC, Eduardo Cabello, Vigo, Spain, [3]Geological Institute, ETH Zürich, Zürich, Switzerland, [4]Department of Earth Science and Environment, Universidad de Alicante, San Vicent del Raspeig, Spain

Key Points:
- Storage of respired carbon in the east equatorial Pacific from interglacial MIS 23 to glacial MIS 22
- Ventilation of the deep sea and inferred atmospheric CO_2 release extended from the end of glacial MIS 22 to full interglacial MIS 21

Supporting Information:
- Supporting Information S1

Correspondence to:
P. Diz,
pauladiz@uvigo.es

Citation:
Diz, P., Cobelo-García, A., Hernández-Almeida, I., Corbí, H., & Bernasconi, S. M. (2020). Persistent east equatorial Pacific carbon storage at the Middle Pleistocene Transition. *Paleoceanography and Paleoclimatology*, *35*, e2019PA003789. https://doi.org/10.1029/2019PA003789

Received 15 OCT 2019
Accepted 24 APR 2020
Accepted article online 9 MAY 2020

Abstract The Middle Pleistocene Transition (MPT, ~641–920 ka) represents a period of the Quaternary climate when, in the absence of substantial changes in orbital forcing, the climate progressively shifted to the 100 ka asymmetrical glacial–interglacial cyclicity characterizing the current climate. The causes of this change remain still uncertain but several lines of evidence suggested the carbon storage of the deep ocean played a relevant role. Here we evaluate the contribution of the eastern deep tropical Pacific to the global ocean carbon sequestration and storage between 760 and 1,040 ka. We present multi-proxy records for export production and the redox environment at the seabed from Ocean Drilling Program Site 1242 located in the deep East Equatorial Pacific. Our data indicate the development of suboxic bottom waters during early marine isotopic stage (MIS) 23 and glacial MIS 22, suggesting the capture and storage of respired carbon. Redox-sensitive elements suggest the progressive oxygenation of the deep ocean initiated at the end of the glacial MIS 22, continued across deglaciation and ended with the accomplishment of full interglacial MIS 21. We describe this pattern as a "less complete deglacial ventilation" in that it differs from the mid-late Pleistocene Pacific deep ocean ventilation pattern which occurs during deglaciations. The ventilation of the deep Pacific Ocean extending beyond deglaciation might have contributed to a persistent deep ocean carbon sequestration, which might have resulted in lowered atmospheric CO_2 values that could have influenced the internal response of the climate system contributing to the development of the 100 ka climate variability.

1. Introduction

The Middle Pleistocene Transition (MPT) represents a period in the Quaternary climate when climate cyclicity changed from short and mild glacial–interglacial 41 ka cycles (pre-MPT,> ~920 ka) to longer, asymmetrical 100 ka ones (post-MPT; <~641 ka, Hughes & Gibbard, 2018). The change in the dominant cyclicity took place in the absence of substantial changes in the orbital parameters (Raymo & Nisancioglu, 2003). Although the underlying mechanisms behind the switch of periodicity remain still unresolved, it appears that the complex interplay of climate-ice sheet dynamics, such as the changes in the removal of regolith beneath the Northern Hemisphere ice sheet (Clark et al., 2006), changes in ocean circulation involving reduction in the thermohaline circulation (Farmer et al., 2019; Pena & Goldstein, 2014), deep ocean cooling (Tziperman & Gildor, 2003) and CO_2 climate feedbacks (Chalk et al., 2017; McClymont et al., 2013) are involved. Reconstructions from boron isotopes (Chalk et al., 2017; Hönisch et al., 2009) and models (Chalk et al., 2017; Köhler & Bintaja, 2008; Lisiecki, 2010a) show a significant drop in atmospheric CO_2 around the time of marine isotopic stage (MIS) 22-MIS 24. In this context, the ocean—as the largest reservoir of carbon exchanging with the atmosphere on glacial and interglacial time scales (Sigman et al., 2010)—might hold a key role in the onset of the 100 ka cycles. Different proxy records suggest increased glacial carbon storage in deep waters of the North Atlantic (Chalk et al., 2017; Lear et al., 2016) and South Atlantic (Farmer et al., 2019) oceans during the MPT, which might have contributed to CO_2 drawdown. So far, the contribution of the tropical Pacific Ocean to the MPT carbon storage is poorly known. Low-resolution studies provide equivocal interpretations of the changes in the equatorial Pacific export production. Murray et al. (2000) showed increased export production in the Deep Central Pacific during the MPT whereas Liu and Herbert (2004) using alkenones, Ma et al. (2015) using barite concentrations and Diester-Haass et al. (2018) using benthic foraminifera abundances did not observe substantial changes in paleoproductivity proxies across the MPT (~500–1,000 ka). Little is known about the oxygenation of the East Equatorial Pacific (EEP) deep waters during the MPT.

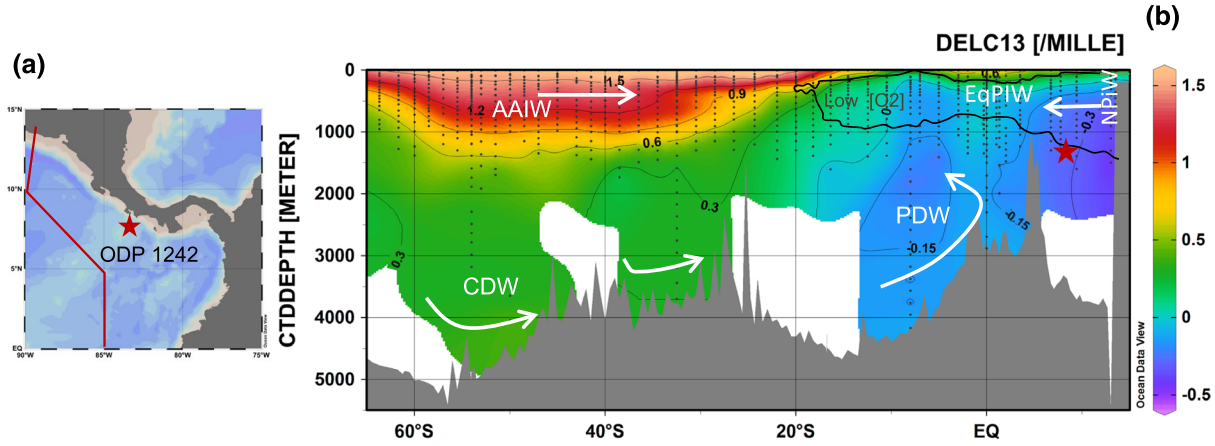

FIGURE 1. Location of ODP Site 1242 and water masses. (a) Location of ODP core Site 1242 (red star) and (b) meridional hydrographic section of $\delta^{13}C_{DIC}$ (Section P19 of PACIFICA database, red line). The bathymetric chart of the N-S section of the East Equatorial Pacific (b) is plotted together with the modern $\delta^{13}C_{DIC}$ distribution (Suzuki et al., 2013). The different signature of the $\delta^{13}C_{DIC}$ water masses in the Pacific Ocean (b) makes $\delta^{13}C_{Cib}$ a good proxy for tracing past ocean circulation (Bostock et al., 2010). The main water masses are PDW (Pacific Deep Water), EqPIW (Equatorial Pacific Intermediate Water); CDW (Circumpolar Deep Water); AAIW (Antarctic Intermediate Water), NPIW (North Pacific Intermediate Waters). Arrows indicate the circulation patterns of the main water masses following the scheme suggested by Talley (2013) and the black line delineates the isopleth of 50 μmol/kg of dissolved oxygen. The Site 1242 is currently bathed by remnants of the northern sourced Northern Pacific Intermediate Water and the Equatorial Pacific Intermediate Water. These figures are generated with Ocean Data View (Schlitzer, R., http://odv.awi.de).

However, several studies focused on the last glacial cycle in the EEP suggested an increase in the storage of glacial respired carbon (Anderson et al., 2019; Bradtmiller et al., 2010; Hoogakker et al., 2018; Jacobel et al., 2017; Umling et al., 2018). The deglacial deep EEP ventilation (de la Fuente et al., 2015; Loveley et al., 2017; Umling & Thunell, 2017) led to the outgassing of the stored respired carbon (Martinez-Boti et al., 2015) thus contributing to modulation of atmospheric CO_2. Here, we present multi-proxy records from the Ocean Drilling Program (ODP) Leg 202 core Site 1242 (Mix et al., 2003) located offshore Costa Rica margin in the eastern equatorial Pacific (Figure 1). The high-sedimentation rates of the Site 1242 allow us to obtain detailed records of changes in the biological pump combining multiple proxies for seafloor oxygenation (redox-sensitive elements) and organic and inorganic production (organic and inorganic carbon concentrations, foraminifera abundance, and isotopes) during the MPT. We provide data that support that the deep EEP stored respired carbon during MIS 23–22 and that the mechanisms by which the carbon is released to the atmosphere might be relevant to understand the contribution of the low-latitude ocean to the modulation of the atmospheric CO_2 and Pleistocene climate variability.

2. Materials and Methods

2.1. Site 1242 and Samples

The ODP Site 1242 (7°51.352′N, 83°36.418′W, 1,364 m water depth, Figure 1a) was retrieved during ODP expedition 202 offshore Costa Rica in the east equatorial Pacific (Mix et al., 2003). The site is on a graben on the crest of the Cocos Ridge bathed at present by remnants of the northern sourced Northern Pacific Intermediate Water and the Equatorial Pacific Intermediate Water (Figure 1b), which is a combination of southern-sourced Antarctic Intermediate Water and Pacific Deep Water (PDW) (Bostock et al., 2010). The site locates underneath the oxygen minimum zone (OMZ) which at present extends from about 200 to 600 m (Stramma et al., 2010). We used the splice record and biostratigraphic data provided by the expedition report (Mix et al., 2003) to obtain samples (1 cm of thickness) at 5 cm intervals between 89 and 125 m composite depth (mcd). The sediments are described as hemipelagic, homogeneous olive green nannofossil clays and clayed nannofossil oozes (Mix et al., 2003). Four tephra layers from Poás and Barva volcanic complexes (Schindlbeck et al., 2016) are identified within the set of samples (Mix et al., 2003, their Table 9; section 2.6 and Supporting information). The sediment samples of ~4 cc were dried, weighed and sieved to 63 μm size fractions and then weighed again after drying (45°C). Samples were analyzed for benthic foraminiferal oxygen and carbon isotopes, bulk sediment organic and inorganic carbon content, major and trace elements, and the abundance and fragmentation of planktic foraminifera.

2.2. Benthic Foraminiferal Isotopes and Age Model

The age model of the ODP Site 1242 is based on the graphical correlation of the benthic foraminiferal oxygen isotope ($\delta^{18}O$ of *Uvigerina auberiana*) record (Diz et al., 2020) to the global benthic $\delta^{18}O$ stack of Lisiecki and Raymo (2005, LR04). A full description of the age model construction can be found in (Diz et al., 2020). In this study, we produced a high-resolution record of benthic foraminiferal carbon isotopes in the shallow infaunal species *U. auberiana* and a low-resolution record of the epifaunal *Cibicidoides* spp. Between two and three well-preserved individuals of *U. auberiana* from the 250–350 μm were used for carbon isotopic measurements. The species *U. auberiana* was nearly absent from the interval between 114 and 115 mcd except for a few samples that depict the deglaciation from MIS 26 into MIS 25. In order to record the deglaciation with a larger number of samples, we used the oxygen isotopic composition of 15 samples from *Melonis barleeanus* in that interval. We measured between five to six individuals from the 250–350 μm fraction of *M. barleeanus* for isotopic measurements. The $\delta^{18}O$ offset between *Uvigerina* and *Melonis* is calculated from six paired sample measurements. The average $\delta^{18}O$ *U. auberiana–M. barleeanus* value was 0.62 ± 0.16‰ (which is comparable to the mean $\delta^{18}O$ offset of 0.55 ± 0.37‰ between *U. peregrina* and *M. barleeanus* indicated by Hoogakker et al. (2010). We added the mean offset to $\delta^{18}O$ *M. baarleanus* values to adjust these values to the $\delta^{18}O$ *U. auberiana* record. Epifaunal benthic foraminifera are scarce in Site 1242 and thus we obtained a medium to low-resolution stable isotopic record. For isotopic analysis, we measured single individuals from the >350 μm fraction of *Cibicidoides* (*C. mundulus* or *C. wuellerstorfi*) or two individuals of each from the >300 μm fraction. The stable isotopes on benthic foraminifera were measured using a GasBench II coupled to a Delta V mass spectrometer as described in Breitenbach and Bernasconi (2011). Foraminifera were placed in vials and reacted with 104% phosphoric acid at 70°C. The instrument was calibrated with the internal standards MS2 ($\delta^{13}C = +2.13‰$, $\delta^{18}O = -1.81‰$) and ETH-4 ($\delta^{13}C = -10.19‰$, $\delta^{18}O = -18.71‰$) which are calibrated to the international reference materials NBS 19 ($\delta^{13}C = +1.95‰$, $\delta^{18}O = -2.2‰$) and NBS 18 ($\delta^{13}C = -5.01‰$, $\delta^{18}O = -23.00‰$; Bernasconi et al., 2018). Values are reported in the conventional delta notation with respect to Vienna PeeDee Belemnite (VPDB). Long-term reproducibility is better than 0.1‰ for both carbon and oxygen isotopes.

2.3. Bulk Sediment Organic and Inorganic Carbon Content

We measured the total inorganic carbon (TIC) content and total organic carbon (TOC) of the sediment at intervals between ~10 and 20 cm. Total bulk sediment samples were dried at 45°C, ground and homogenized using a zircon ball mill. The weight percentage of carbon was measured using a macro elemental analyzer LECO CNS2000 in the UVIGO Research Unit Services (CACTI) and is reported in weight percent. We calculated the TIC as the difference between the total carbon content of an untreated sample and that of an aliquot of the sample heated at 400°C for 3 h to remove organic carbon. The TOC content is used here, and it is available in Diz et al. (2020). The inorganic carbon content (TIC) provides information about the carbonate production but also the potential influence of carbonate dissolution by corrosive bottom waters (e.g., Sexton & Barker, 2012, see discussion section). The TOC is used here as a qualitative proxy for the supply of organic carbon to the seafloor (e.g., Schoepfer et al., 2015, see discussion).

2.4. Major and Trace Elements (Al, Ca, Sr, Mn, U, Th and Rare Earth Elements)

We evaluated sediment composition, paleoxygenation conditions, and provenance from the quantification of bulk sediment elemental concentrations of major (Al, Ca) and trace elements (Mn, Sr, U, Th, and rare earth elements [REE]). Dried samples (~50 mg) were weighed and transferred to screw-capped PFA vessels (Savillex). Then, we added 3 mL of concentrated HF, 3 mL of concentrated HNO_3 and 1 mL of concentrated HCl and the samples were digested at 195°C for 24 h using a Teflon-coated (PicoTrace) hot plate. Due to the formation of insoluble fluorides for several elements (e.g., REE, Th), we added boric acid after digestion and heated at 195°C for 2 h. Digested samples were then diluted to 50 mL with MQ water, and analyzed using external calibration. The elemental determination was carried out using an Agilent 7900 ICPMS. The monitored isotopes and the target elements were the following: ^{27}Al, ^{43}Ca, ^{44}Ca, ^{55}Mn, ^{88}Sr,^{232}Th, ^{238}U, and the REE; ^{139}La, ^{140}Ce, ^{141}Pr, ^{146}Nd, ^{147}Sm, ^{153}Eu, ^{157}Gd, ^{159}Tb, ^{163}Dy, ^{165}Ho, ^{166}Er, ^{169}Tm, ^{172}Yb, and ^{175}Lu. The elements Al, Ca, Mn, and Sr were analyzed in the He collision mode in order to minimize the impact of spectral interferences in their determination. Potential interferences from oxides, argide, and doubly charged species were monitored and accounted for when necessary. Appropriate amounts of Ge, In, and Ir were

spiked to the samples and used as internal standards monitoring the isotopes ^{72}Ge, ^{115}In, and ^{193}Ir to account for instrumental drift and matrix effects. Accuracy was checked by means of the analysis of a marine sediment certified reference material (MESS-3; NRC, Canada), obtaining recoveries ranging from ~80% (e.g., Al, Mn) to ~100% (e.g., REE). Precision was generally below 5%.

2.5. Redox-Sensitive Metals: Proxies for Paleoxygenation at the Sediment–Water Interface

Obtaining a reliable reconstruction of deep ocean oxygen conditions is challenging because of the uncertainties that could potentially affect the proxies used for that purpose (Tribovillard et al., 2006). We proceed by using a multi-proxy approach to compensate specific limitations associated to individual proxies. Thus, we used a combination of redox geochemical proxies; manganese, authigenic uranium and the cerium anomaly to infer changes in the oxygenation at the seabed. The Mn/Th ratios were used to infer past qualitative oxygenation levels in the sediments (see Figure S1). Thorium was used for normalization purposes as it can be used as a conservative lithogenic element because of its low solubility and its limited reactivity (Larrose et al., 2010). The underlying assumption was that Mn (II), which is more soluble than Mn (IV), is released to the porewaters as a result of reductive dissolution of oxyhydroxide particles occurring under oxygen-depleted settings. In oxygen-enriched settings, Mn precipitates in the form of insoluble oxyhydroxides. Thus, Mn (Mn/Th) is expected to decrease under reducing conditions and increase under well-oxygenated environments. Because Mn can be very mobile in reducing sediments (Tribovillard et al., 2006), interpretation of redox conditions should not be based solely on the Mn/Th but should be supported by other redox-sensitive metals such as authigenic uranium (aU) and the cerium anomaly (Ce*).

Uranium is present as U (VI) in oxygenated settings in the form of a soluble uranyl carbonate. The reduction of soluble U (VI) to insoluble U (IV) occurs under redox conditions near the conversion of Fe (III) to Fe (II) (i.e., suboxic conditions) (Morford & Emerson, 1999), which is mediated by bacteria. This process favors the diffusion of the soluble carbonate uranyl from the overlying water column to the porewater, where authigenic uranium precipitates in the form of oxides in the sediment (Tribovillard et al., 2006). We calculated the authigenic fraction of uranium (aU) in the sediment by subtracting the detrital U fraction from the total U measured as follows: with authigenic U (aU) = $U_{measured} - U_{detrital}$ being $U_{detrital}$ = U/Th (upper continental crust) *$Th_{measured}$. We took the U and Th values for the calculation of $U_{detrital}$ (U/Th = 0.257) from the upper continental crust values of Rudnick and Gao (2014).

Cerium is one of the REE relevant for tracing redox processes. Cerium is unique, as unlike other REE which are stable under the III form, it shows two oxidations states: the Ce (III) which is highly soluble and the insoluble Ce (IV) state. Thus, Ce may show anomalies (expressed as Ce*) due to the oxidation or reduction processes being a potential tracer of past sedimentary oxygenation state (De Baar et al., 1985; German & Elderfield, 1990). Thus, in oxygenated conditions, soluble Ce (III) is oxidized to insoluble Ce (IV), and bulk marine sediments should show a positive anomaly (≥1). Under suboxic or anoxic conditions the removal of insoluble Ce (IV) (which is reduced to soluble Ce (III)) yields sedimentary negative anomalies (<1) (Pattan et al., 2017). Some studies suggest that whereas the absence of cerium anomaly might be inconclusive for identifying redox conditions, if present, it provides a robust indication of the oxygen conditions of the environment (Tostevin et al., 2016). In this study, we measured Ce in bulk sediments and use the definition of Ce* provided by Dubinin (2004),also used by other authors (Haley et al., 2004), that includes normalization of Ce calculated to the neighbor elements La y Pr, as follows: $Ce^* = 2^*(Ce/Ce^{NASC})/(La/La^{NASC} + Pr/Pr^{NASC})$. NASC values were taken from Dubinin (2004).

2.6. Dispersed Ash and its Potential Influence in the Bulk Elemental Composition of the Sediments

Four tephra layers were identified within the set of samples (Mix et al., 2003, their table 9). Two of them are 1–2 cm thick and were found at 95.05 and 115.48 mcd and the other two are 15 cm thick and found at 103.99–104.13 mcd and 108.56–108.70 mcd. We observed glass particles in the >125–63 μm fraction of the sediments deposited after the sedimentation of the discrete tephra layers. This volcanic material could be described as "dispersed ash" as defined by Scudder et al. (2016) and might compromise geochemical interpretations based on elemental concentrations. Geochemical measurements suspected to be affected by volcanic should not be used to infer paleoenvironments. Consequently, and in order to obtain an end-member elemental composition for the volcanic material, we measured the composition of REE and Th within described tephra layers.

In particular, we measured one sample from the marine tephra layer described by Mix et al. (2003) between 103.99 and 104.13 mcd (sample 202-1242A-11H-3, 115–116 cm, 104.08 mcd) and two samples from the tephra layer described between 108.56 and 108.70 mcd (samples 202-1242C-11H-3-120-121, 180.6 mcd; and 202-1242C-11H-3-130-131, 108.7 mcd). We used the concentration of ∑REE and the relation of light REEs (LREEs) to heavy REEs (HREEs) and Th concentrations to characterize the influence of volcanic material outside the deposition of the tephra layer, that is, the dispersed ash. We used the LREE/HREE formula and the NASC values indicated in Dubinin (2004):

$(LREE/HREE)^{NASC} = (La/La^{NASC} + 2\ Pr/Pr^{NASC} + Nd/Nd^{NASC})/(Er/Er^{NASC} + Tm/Tm^{NASC} + Yb/Yb^{NASC} + Lu/Lu^{NASC})$. We complemented our geochemical interpretation with the physical properties measurements obtained by Mix et al. (2003). Samples embracing anomalously high concentrations of Th and REEs are considered "contaminated" (i.e., influenced by volcanic) and discharged from the discussion. Following this approach, we removed 40 geochemical samples (see Figure S2 and data availability statement).

2.7. Planktonic Foraminifera Counts

The abundance of planktonic foraminifera and the fragmentation are used here to evaluate the significance of the carbonate records (carbonate production vs. dissolution). We calculated the abundance of planktonic foraminifera at 60 cm intervals (120 samples). We counted a representative split of at least 100 whole planktonic foraminifera from the >150 μm size fraction to calculate the abundance of whole planktonic individuals per gram of dry weight sediment (P.F./g). The amount of planktonic foraminiferal fragments in each split is also counted, and the percent of fragmentation is calculated. The fragmentation index of Le and Shackleton (1992) is used (%Fragmentation = 100* ((number of fragments/8)/(number of fragments/8 + number of whole)) as a proxy for corrosiveness of the bottom waters to calcium carbonate.

3. Results

3.1. Epifaunal and Infaunal $\delta^{13}C$ Records of Site 1242

The moderate resolution epifaunal record of *Cibicidoides* spp. ($\delta^{13}C_{Cib}$) shows values ranging from near 0‰ at late MIS 21 to values as low as −1‰ during MIS 23, 22, and 20 (Figure 2c). The average difference between paired $\delta^{13}C$ measurements of *Cibicidoides* spp. and the infaunal *U. auberiana* ($\Delta\delta^{13}C_{Cib\text{-}Uvi}$) was 0.72 ± 0.33‰ ($n = 55$). However, the $\Delta\delta^{13}C_{Cib\text{-}Uvi}$ showed values lower than the average before 930 ka (0.41 ± 0.24‰, $n = 13$). This finding, together with the fact of *U. auberiana* is an infaunal species with a variable microhabitat (Licari et al., 2003), precludes using a constant correction factor to convert $\delta^{13}C_{Uvi}$ values to the $\delta^{13}C_{Cib}$ scale. Thus, we considered $\delta^{13}C_{Cib}$ to mainly track the $\delta^{13}C_{DIC}$ of bottom waters (Schmittner et al., 2017) and $\delta^{13}C_{Uvi}$ to record information about the $\delta^{13}C_{DIC}$ of pore waters, which depends on the $\delta^{13}C_{DIC}$ of bottom waters and the respiration processes occurring in the first centimeters of the sediment (Mackensen & Schmiedl, 2019).

3.2. Total Organic and Inorganic Carbon Records

The supply of organic carbon to the seafloor is estimated by the TOC and the organic matter remineralization in pore waters by $\delta^{13}C_{Uvi}$. The TOC of Site 1242 is relatively high with values generally above 1% (Figure 2d). The pattern of high-glacial and low-interglacial accumulation of organic matter initiates at ~920 ka (Figures 2 and 3d). High values of TOC occur during early MIS 23 and glacials MIS 22 and 20 (Figure 3d). High TOC and depleted $\delta^{13}C_{Uvi}$ values are observed in glacial periods, particularly those after 920 ka (Figures 2b and 2d). In particular, early MIS 23 is characterized by an abrupt drop in $\delta^{13}C_{Uvi}$ of about 0.7‰ lasting for about 10 ka (Figure 2b), suggesting intense organic carbon remineralization in the pore waters.

The deep-sea carbonate chemistry is interpreted by multiple proxy records such as TIC, the Ca/Al and Sr/Al ratios and the abundance and fragmentation of planktic foraminifera (Figures 3b, 3e, and 3f). The pattern of high-glacial values of TIC and Ca-related proxies (Ca/Al, Sr/Al) and the abundances of planktic foraminiferal characterizes all glacial periods, but increased values occurred after ~920 ka (Figure 3). The record of percent fragmentation does not show glacial–interglacial variability (Figure 3c). The addition of volcanic ash from the deposition of the tephra layer at MIS 24 and middle MIS 23 influences the records of TOC

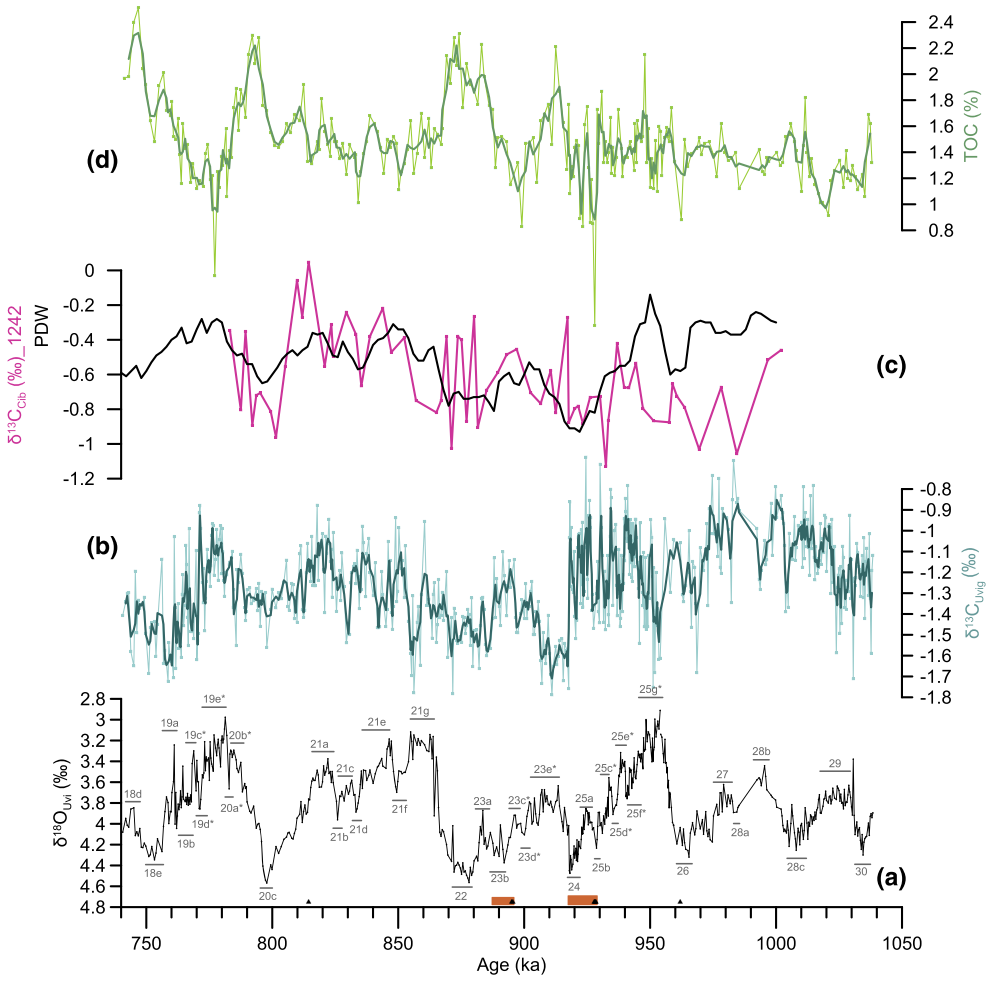

FIGURE 2. Carbon isotope composition of infaunal and epifaunal benthic foraminifera. Record of benthic oxygen isotopes (a), data from Diz et al. (2020). Numbers indicate the marine isotopic stages. The suborbital climate variability is indicated with a letter following the normal alphabetic order, convention proposed by Railsback et al. (2015). The tentative location of new substages is indicated by "*". The high-resolution record of the infaunal benthic foraminifera *Uvigerina auberiana* ($\delta^{13}C_{Uvig}$) is represented in (b) and the thick dark green line is the three points running average. The moderate resolution curve of the epifaunal benthic foraminera *Cibicidoides* spp. ($\delta^{13}C_{Cib}$) is represented in (c, pink line), and it is compared with the Pacific Deep Water (PDW, black line) stack integrating the $\delta^{13}C$ of *Cibicidoides* spp. records of EEP of ODP sites 849, 846, 677, and 806 located at depth > 2,500 m (black line) (Martínez-Méndez et al., 2013). The total organic carbon content of the sediments (TOC) is indicated in (d). The thick green line represents the three points running average. Horizontal orange bars at the bottom of *x*-axis indicate the influence of dispersed ash.

and calcium carbonate related proxies which show punctual depletions (Figure 3). Some of the variability showed by TIC and TOC might be influenced by the incorporation non carbonate components causing dilution during interglacials when sedimentation rates increases (see Figure S3).

3.3. Paleoxygenation From Redox-Sensitive Elements

Elevated aU concentrations (>3 ppm) are found at glacials MIS 26, 22, and 20 and early stages of MIS 23 (Figure 4b) with the highest aU values of the whole record, up to 7 ppm, observed during full glacial MIS 22. This occurs in coincidence with low Mn/Th (Figures 4b and 4c) and the highest negative Cerium anomaly (Ce*, Figure 4d) suggesting suboxia at the sediment–water interface. Other intervals showing a highly negative Ce* are early MIS 23 and glacials MIS 26 and MIS 20. The deglaciations are characterized by large decreasing trends in aU concentrations and increasing Mn/Th ratios and Ce* (Figure 4, green bars). The lowest aU values (~1.5 ppm) occur during interglacial maxima of MIS 25 and MIS 21 (Figure 4b) in coincidence

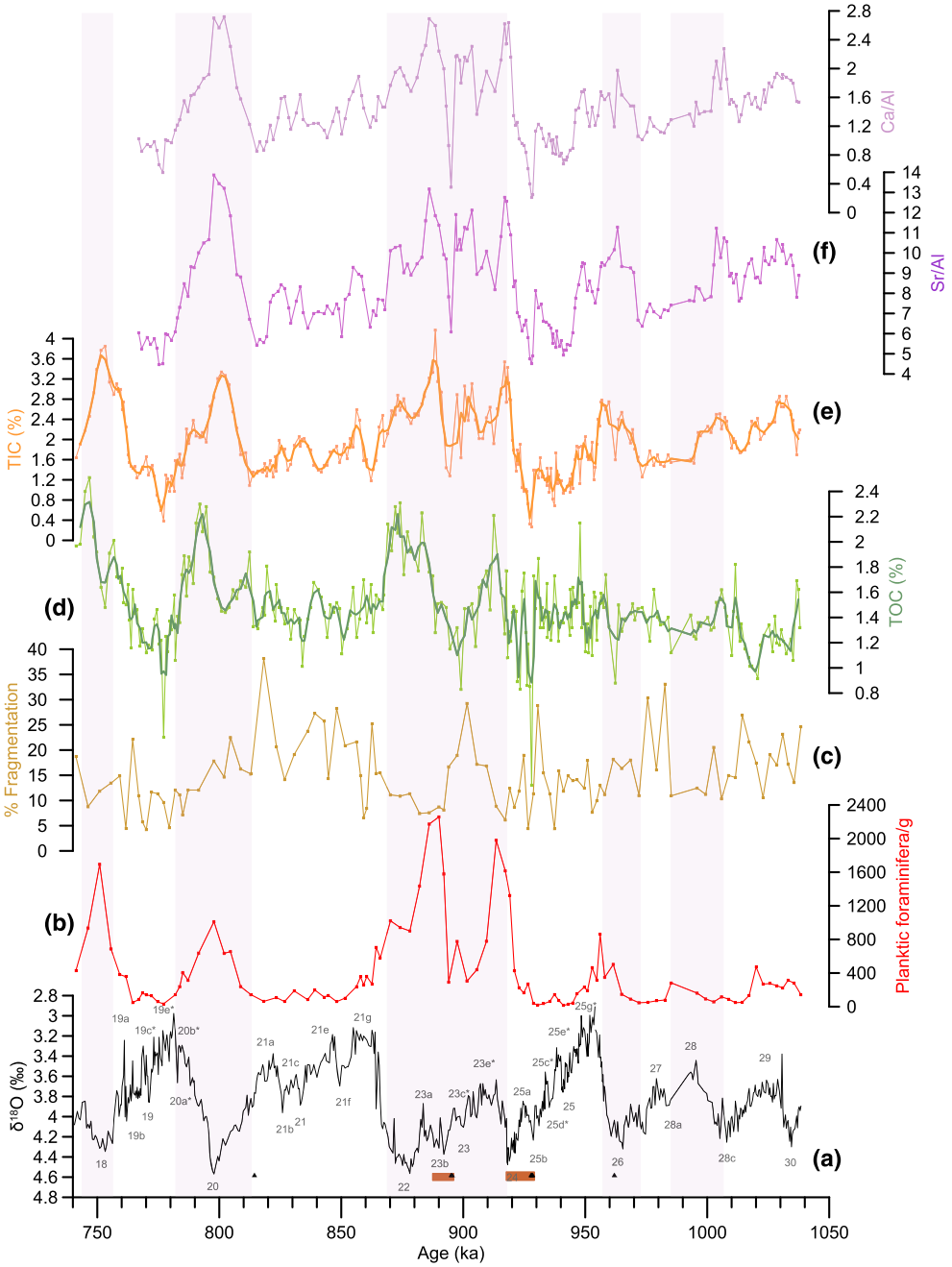

FIGURE 3. Organic and inorganic carbon variability. Record of benthic oxygen isotopes and horizontal orange bars (a) as in Figure 2. The abundance of planktic foraminifera (b), the fragmentation index (c), TOC (d), TIC (e), and calcium-related proxies (Ca/Al, Sr/Al, f) are plotted together to show the correspondence between carbonate related proxies (e–f), planktic foraminiferal abundance (b) and organic carbon (d) suggesting the contribution of surface ocean carbonated production to deep-sea carbonate variability.

with high Mn/Th ratios (Figure 4c) suggesting an oxygenated sedimentary environment at the sediment–water interface and pore waters.

Post-depositional alteration (burndown) might influence aU concentrations of Pacific sediments (Jacobel et al., 2017; Jacobel et al., 2020; Mills et al., 2010). It might be argued that glacial MIS 22 peak of aU is the result of U burndown by the increased influence of high-oxygenated bottom waters to the core site during the subsequent interglacial. However, if post-depositional, remobilization influenced aU should equally

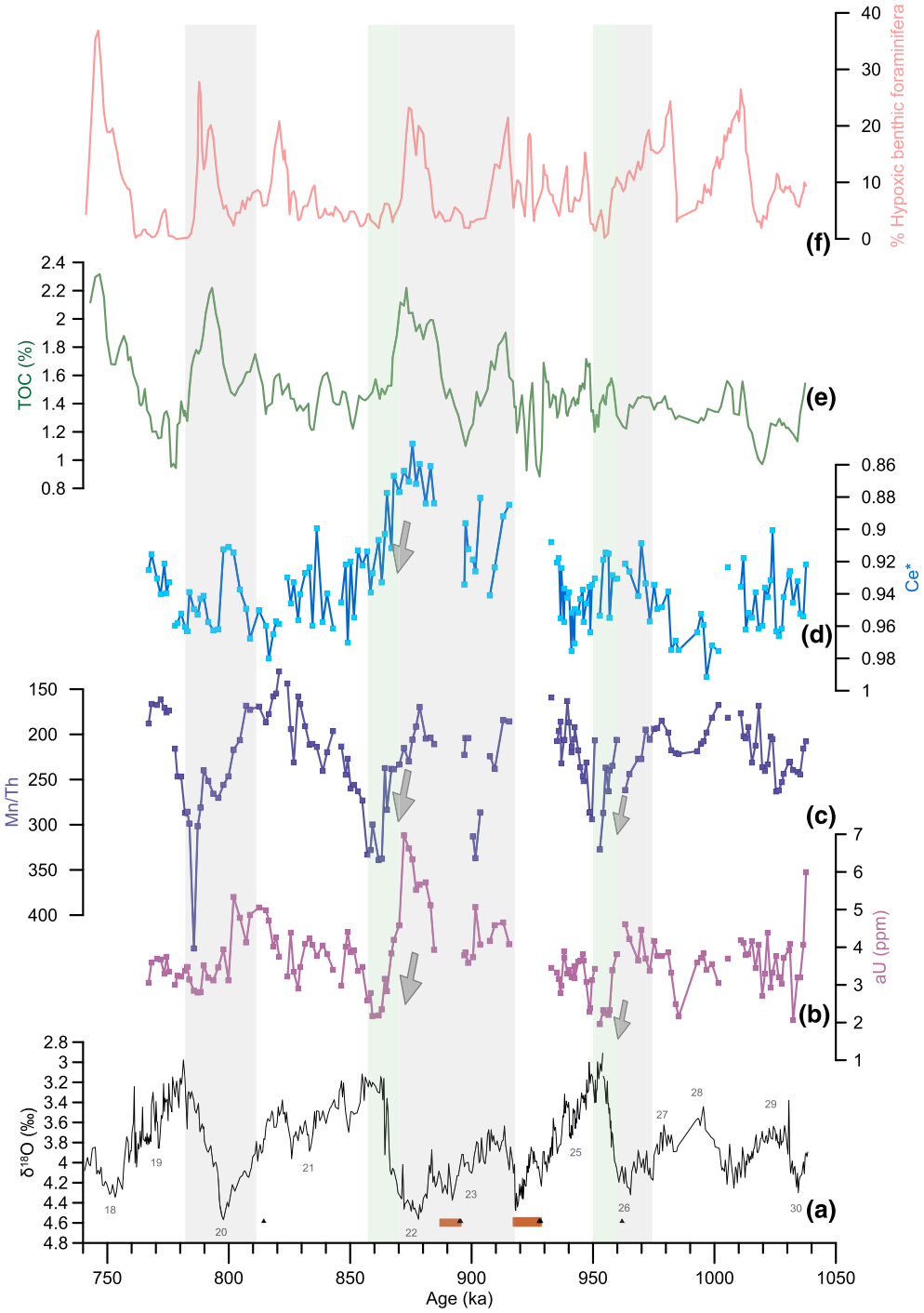

FIGURE 4. Paleoxygenation in Site 1242. Record of benthic oxygen isotopes and horizontal orange bars (a) as in Figure 2. Proxies for the oxygen concentration in the bottom waters (b–d) are compared with proxies for the organic production (e) to give an indication of the role of the East Equatorial Pacific in capturing and sequestering carbon during the MPT. Redox-sensitive elements are the authigenic uranium-aU (b); Mn/Th ratios (reversed *y*-axis, c) and cerium anomaly Ce*(reversed *y*-axis, d). Gray arrows and green bars indicate progressive ventilation of the deep sea. The percentage of benthic foraminiferal species representative of intermediate and severe hypoxia in the bottom waters (Diz et al., 2020) are indicated in (f). Data from redox-sensitive elements influenced by volcanic material are removed from the discussion, and data are not represented (see methods and Supporting Information Figure S2 and data availability statement).

affect Mn deposition (a highly mobile element) and other redox elements (Ce*). Authigenic uranium has the opposite behavior across deglaciation to Mn/Th and Ce* suggesting that post-depositional mobilization of trace elements is unlikely. Additionally, sedimentation rates are high (>10 cm/ka, Figure S3) enough to minimize bioturbation and post-depositional remobilization of aU (and the other redox-sensitive elements). The variability shown by aU concentrations do not seem to be determined by changes in the sediment accumulation (see Figure S3).

4. Discussion

4.1. Water Mass Structure of Site 1242 During the MPT

The different signature of the $\delta^{13}C_{DIC}$ of intermediate and deep water masses in the Pacific Ocean (Figure 1) makes the carbon isotopic record of epifaunal benthic foraminifera a good proxy for tracing past ocean circulation (Bostock et al., 2010). We compare the low-resolution record of the carbon isotopic composition of epifaunal benthic foraminifera *Cibicidoides* spp. ($\delta^{13}C_{Cib.}$) to other Pacific records to provide a perspective on the vertical water mass structure during the MPT. The record of $\delta^{13}C_{Cib}$ of Site 1242 contains similar carbon isotope signals and glacial–interglacial variability to the *Cibicidoides* spp. $\delta^{13}C$ stack for the PDW (named after that $\delta^{13}C_{PDW}$) (Martínez-Méndez et al., 2013) from 930 to 780 ka (Figure 2c). The stack was constructed by a compilation of $\delta^{13}C$ measurements of *Cibicidoides* spp. from East Equatorial Pacific deep Sea cores, and it is considered a good representation of $\delta^{13}C$ values for water depths deeper than 2,500 m in the Equatorial deep Pacific for the last 1 Ma (Lisiecki, 2010b; Martínez-Méndez et al., 2013). The striking similarity between $\delta^{13}C$ signatures and variability patterns between both records (Figure 2, see also Text S1 and Figure S4 for further support) suggests the influence of the PDW over Site 1242 for most of the record. For this reason, we consider our interpretations for Site 1242 to be representative of the characteristics of the deep tropical East Pacific waters.

4.2. Interpretation of changes in the organic and inorganic carbon content at the MPT

The record of TIC (and Ca-related proxies) shows the so-called "Pacific style" (Sexton & Barker, 2012) pattern of high values during glacials and low values during interglacials. The factors explaining EEP deep water carbonate variability are still under debate with studies indicating Late Pleistocene carbonate productivity as the main driver (Diz et al., 2018; Thomas et al., 2000) and others focusing on deep water carbonate chemistry (i.e., dissolution) (Farrell & Prell, 1989; Sexton & Barker, 2012). Site 1242 is well above the depth of modern (Thunell et al., 1981) and Late Pleistocene lysocline (López-Otálvaro et al., 2008). Dissolution evaluated from coccolith abundance and species composition at Site 1242 indicates good to moderate preservation (López-Otálvaro et al., 2019) during the MPT. The correspondence between TIC, Ca-related proxies (Ca/Al, Sr/Al), the abundance of planktonic foraminifera, and the lack of clear trend in fragmentation values (Figure 3) suggests minor influence of $CaCO_3$-undersaturated deep waters. These results suggest that calcium carbonate productivity in surface waters (mainly from planktonic foraminifera and coccoliths) play a major role explaining the inorganic carbon variability at Site 1242. Low TIC values during interglacials (in particular MIS 25) compared to glacials might be influenced by dilution (high-sedimentation rates of noncarbonate components). The slight offset observed between peaks of TIC and TOC during glacials/terminations (i.e., TIC starts to decrease when TOC reaches maximum concentrations, Figures 3d and 3e) could be a attributed to supralysoclinal carbonate dissolution caused by carbonate undersaturation in the pore waters by the remineralization of high amounts of exported organic matter (Peterson & Prell, 1985).

The early MIS 23 (~920 ka) marks the beginning of the large fluctuations in both TOC and calcium carbonate-related proxies with high values during glacials and low values during interglacials (Figure 3). This pattern might suggest a coupling between organic and inorganic production over the study period. However, some other factors might have played a role in shaping the organic carbon variability. Increased TOC coincide with $\delta^{13}C_{Uvi}$ depleted values (Figures 2b and 2d). In particular, early MIS 23 is characterized by an abrupt drop in $\delta^{13}C_{Uvi}$ when the $\delta^{13}C$ values reach for the first time values as low as −1.75‰. Those values are comparable to the glacial depleted values observed in the EEP Pacific during the mid-late Pleistocene (Figure S5). The correspondence between TOC and $\delta^{13}C_{Uvi}$ potentially links increase of organic carbon supply to the seafloor to organic matter remineralization in pore waters (Figure 2). However, remineralization rates in pores waters are controlled by deep-water oxygen and organic carbon fluxes

(Mackensen & Schmiedl, 2019). The detailed analysis of benthic foraminifera in Site 1242 reveals that peaks of TOC, in particular those during early MIS 23 and MIS 22, occur in coincidence with the presence of species related to sustained productivity and the appearance of benthic foraminifera characteristic of intermediate hypoxic conditions in bottom waters (Figures 4e and 4f). This correspondence suggests that peaks in TOC cannot be solely related to increased organic export production, but they could also respond to enhanced preservation which occurs when the exposure of organic material to oxygen is minimized through reducing bottom-water conditions and high-sedimentation rates (Schoepfer et al., 2015).

4.3. Storage of Respired Carbon During Mild Interglacial MIS 23 and Glacial MIS 22

Increased export production has the potential to enhance carbon sequestration in the deep ocean acting to capture atmospheric CO_2 in the ocean interior (Sigman et al., 2010). As the rain of organic carbon from the surface drives respiration at depth, an increase in oxygen consumption caused by increased export production should be accompanied by a decrease in oxygen concentrations of the deep ocean (Hain et al., 2014; Jacobel et al., 2017). Decreased bottom water ventilation, increasing the residence time of the CO_2 produced by organic matter respiration in the deep ocean, might also contribute to the capture of carbon at the seafloor. Evaluating the changes in the export production together with the oxygen concentration of deep waters gives an indication of the contribution of the biological pump to the carbon sequestered in the deep ocean.

The authigenic uranium (aU) enrichment in the sediments has been long used as a quantitative proxy for bottom water redox state (e.g., Jacobel et al., 2020). However, the analysis of the Late Pleistocene records of aU in the equatorial Pacific indicate that its accumulation is strongly influenced by the flux of organic carbon (Jacobel et al., 2020). The highest enrichment in aU in Site 1242 during glacial MIS 22 appears in concert with a peak in TOC (Figures 4b–4e), which might suggest the contribution of sinking carbon to the aU signal. High concentrations of particulate organic matter and low oxygenation in the water column might favor the formation and preservation of particulate aU (Anderson, 1982) which could contribute to the total aU measured in the sediments (Zheng et al., 2002). The organic enrichment might also contribute to the respiration of organic matter creating reducing conditions that lead to the aU precipitation in the sediment water interface, or the preservation (no dissolution) of the particulated aU deposited in the sediments. Those processes might occur independently of the oxygen concentrations of bottom waters. These findings suggest that in Site 1242, aU cannot be used as a single proxy for a decrease of the oxygen concentrations in the bottom waters. The combined inspection of the record of aU and other redox-sensitive proxies such as Mn/Th and Ce* reveals that the highest aU enrichment is inversely related to Mn/Th and Ce* values during MIS 22. The information provided by those other redox-sensitive proxies suggests depleted oxygen concentrations at the sediment water interface, which could result from the respiration of the organic matter which uses oxygen, but also from a decreased ventilation of the bottom waters (PDW, see section 4.3) advected through the Site 1242, with likely both processes resulting in an effective capture and storage of respired carbon. This interpretation could be extended to the early stages of MIS 23 when proxy records indicated moderately high concentrations of aU in coincidence with oxygen-depleted bottom waters (Figures 4b–4d), increased TOC (Figure 4e), and organic carbon remineralization in pore waters inferred from $\delta^{13}C$ (Figure 2b). The high abundances of benthic foraminiferal species typical of hypoxic conditions support the interpretation provided by geochemical proxies (Figure 4f).

The inference of oxygen depleted environment suggests the sequestration and storage of organic carbon during glacial MIS 22 but also during early mild interglacial MIS 23. The storage of glacial carbon was also inferred for MIS 22 from a record of magnetite dissolution in carbonate free environments of the NW Pacific (Korff et al., 2016). Interestingly, the 1 Ma record of Korff et al. (2016) from 5,100 m water depths does not show large amounts of respired carbon storage during the following glacial stages MIS 20 and 18 as to produce magnetite dissolution. This is also evident in our records that show moderate increases of aU and moderate Ce* depletions during MIS 20. Remarkably, the next glacial period showing lowered oxygen concentrations in the NW Pacific (Korff et al., 2016) and in the EEP (Mills et al., 2010) is MIS 12. This pattern highlights the relevance of the environmental changes occurring during the MIS 22–23/24 (the termed "900 ka event", Clark et al., 2006) for the onset of the dominant 100 ka cycles (McClymont et al., 2013, Pena & Goldstein, 2014; Farmer et al., 2019). The contribution of early MIS 23 to the carbon storage is significant because it seems that mild interglacial MIS 23 behaves "like" a glacial as suggested by other

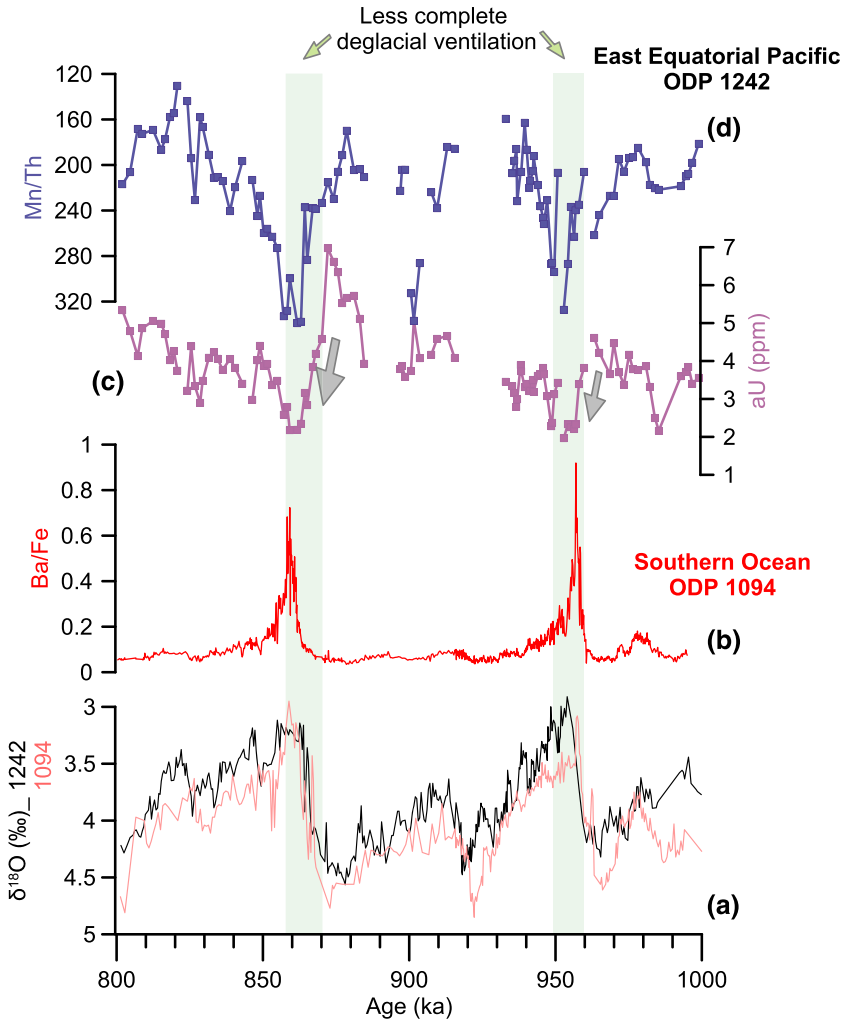

FIGURE 5. "Less complete deglacial ventilation" at Termination X in the East Equatorial Pacific and the Southern Ocean. Benthic oxygen isotopes in ODP Site 1242 in the EEP (black line) and planktonic oxygen isotopes of ODP Site 1094 in the Southern Ocean (pale pink) (Hasenfratz et al., 2019) show an overall temporal consistency between the two independent age models (a). The record of Ba/Fe in the Antarctic sector of the Southern Ocean (ODP 1094, Jaccard et al., 2013) is plotted in the new age model of Hasenfratz et al. (2019) (b). The records of redox-sensitive elements aU (b) and Mn/Th (c) indicate that the oxygenation in bottom waters of Site 1242 begins at the end of glacial MIS 22 (also MIS 26) (aU decreases and Mn/Th increases), continues all the way through the deglaciation and ends up once full interglacial conditions are attained (green vertical bars).

authors (Pena & Goldstein, 2014). The isolation of the respired carbon during the MIS 23–22 interval in the EEP might have acted to effectively lower atmospheric CO2. This finding highlights the contribution of the deep tropical Pacific, and probably other low-latitude areas, to carbon trapping during a key stage of the MPT (MIS 22–23), adding to the evidence shown in other high-latitude regions such as the deep North Pacific (Kender et al., 2018), North Atlantic (Lear et al., 2016), and the South Atlantic (Farmer et al., 2019).

4.4. Less Complete Deglacial Ventilation of the EEP During Termination X

The ventilation of the EEP during the mid-late Pleistocene (de la Fuente et al., 2015; Loveley et al., 2017) is thought to be linked to overturning changes in the Southern Ocean (Umling & Thunell, 2017) through a set of ocean and atmospheric teleconnections occurring at terminations. These processes involve a southward shift in the intertropical convergence zone (Diz et al., 2018; Menviel et al., 2018) and in the Southern Ocean westerlies (Ceppi et al., 2013) and increasing the upwelling of nutrients to the Antarctic zone (Rae et al., 2018) and the invigoration of the ocean tunneling (Spero & Lea, 2002) transporting nutrients to the

EEP thermocline via the Subantarctic mode water or the Antarctic Intermediate Water. The analysis of the set of redox-sensitive elements (aU, Ce* and Mn/Th ratios) presented in this study indicates that the transition from glacial MIS 22 to interglacial MIS 21 describes decreasing aU and increasing Ce* and Mn/Th suggesting a progressive shift from a suboxic sedimentary environment to a well-oxygenated deep ocean (Figures 4b–4d). The ventilation of the seabed across deglaciation is also indicated by the increase in the $\delta^{13}C_{Uvi}$ values (Figure 2b). Interestingly, the peaks in Mn/Th and the high Ce* suggesting full ventilation (i.e., oxygenated conditions) of the seabed do not occur across Termination X but only after having attained full interglacial conditions during MIS 21 (Figure 4, green bars and gray arrows). This pattern suggests a "less complete deglacial ventilation" in comparison to the mid-late Pleistocene when the ventilation of the deep (de la Fuente et al., 2015), intermediate (Loveley et al., 2017), and subthermocline (Umling & Thunell, 2017) EEP and Southern Ocean waters (Rae et al., 2018) occurs at terminations. The description of a less complete ventilation was first indicated by Kemp et al. (2010) in the Antarctic sector of the Southern Ocean for the glacials and interglacials of the MPT. The analysis of the productivity records of the Antarctic sector of the Southern Ocean, indicated by the Ba/Fe ratios (Jaccard et al., 2013), shows that peaks of productivity occurred during interglacial MIS 21 (Figure 5). The pattern is less clear for Termination XI and the interglacial MIS 25. Because the Antarctic productivity relates to the southward shift of the westerlies promoting wind-driven upwelling (Anderson et al., 2009; Jaccard et al., 2013; Rae et al., 2018), the interglacial peak of Ba/Fe represents an indirect indication of less complete deglacial ventilation of the Southern Ocean during Termination X (Figure 5). This scenario might be explained by expanded Antarctic sea ice and the location of the polar front further North, which could have caused a northward shift of the westerlies reducing their ability to fully ventilate the deep ocean during the deglaciation process, thus reducing the upwelling of deep waters (Kemp et al., 2010). The pattern shown by the Ba/Fe record indicates that the less complete deglacial ventilation of TX is not unique to the EEP and it might be extended to the Southern Ocean.

The Southern Ocean and the East Equatorial Pacific are two ocean areas relevant for climate regulation during the late Pleistocene. There are several evidences suggesting that deglacial atmospheric CO_2 outgassing in the Southern Ocean and the East Equatorial Pacific (Martinez-Boti et al., 2015; Rae et al., 2018) might have contributed to deglacial warming aiding to set the process that gives end to the glacial eras (Denton et al., 2010). We hypothesize that the less complete deglacial ventilation of the EEP (and the Southern Ocean) during Termination X might have led to the incomplete release of glacial carbon stored during MIS 23–22 to the atmosphere across the deglaciation into MIS 21. An incomplete outgassing of CO_2 during deglaciation might have favored that the Earth had crossed some sort climate threshold that contributed to drive the Earth progressively into the 100 ka variability. Further research should be carried out to investigate the deglacial mechanisms across the MPT and their linkages to climate variability and the evolution of atmospheric CO_2.

5. Conclusions

This study presents multi-proxy records from the ODP Site 1242 used to investigate changes in the oxygenation of the sedimentary environment of the East Equatorial Pacific during the MPT. Those records are presented together with an exceptional resolution record of benthic foraminifera stable isotopes between 760 and 1,040 ka. We provide evidence for the role of the EEP deep waters in capturing and storing respired carbon during MIS 23–22 (870–920 ka), which probably resulted in lower atmospheric CO_2. The ventilation of the EEP, and thus the release of the carbon stored during glacial MIS 22–23, did not occur mainly during the deglaciation into MIS 21 (as it seems to function during the mid-late Pleistocene terminations), but it was finally accomplished under full interglacial conditions. We suggest that this less complete deglacial ventilation could have retained the carbon stored during the previous interval favoring an incomplete deglacial release of CO_2 to the atmosphere. This process might have induced changes in the internal climate response contributing to the sequence of events involved in the transition to the current mode of climate variability.

Data Availability Statement

Data sets related to this manuscript are archived in Pangaea (https://doi.org/10.1594/PANGAEA.911964)).

Acknowledgments

Authors appreciate the suggestions and comments of Dr. Zunli Lu and an anonymous reviewer which improved the manuscript. Authors would like to thank IODP for providing the sample material used to carry out this study and also the curators of the Green Coast Repository. Authors are grateful to Madalina Jaggi for technical assistance with foraminifera isotope analysis. The laboratory technical assistance of Victor González Guitián to perform elemental analysis was funded by Xunta de Galicia through the program GRC-ED431C 2017/55. This study was funded by the project CGL2016-79878-R (Spanish *Ministerio de Economía, Industria y Competividad* within the state program *Investigación Desarrollo e Innovación Orientada a los Retos de la Sociedad*).

References

Anderson, R. F. (2020). Concentration, vertical flux, and remineralization of particulate uranium in seawater. *Geochimica et Cosmochimica Acta*, *46*(7), 1293–1299. https://doi.org/10.1016/0016-7037(82)90013-8

Anderson, R. F., Ali, S., Bradtmiller, L. I., Nielsen, S. H. H., Fleisher, M. Q., Anderson, B. E., & Burckle, L. H. (2009). Wind-driven upwelling in the Southern Ocean and the deglacial rise in atmospheric CO_2. *Science*, *323*(5920), 1443–1448. https://doi.org/10.1126/science.1167441

Anderson, R. F., Sachs, J. P., Fleisher, M. Q., Allen, K. A., Yu, J., Koutavas, A., & Jaccard, S. L. (2019). Deep-sea oxygen depletion and ocean carbon sequestration during the last ice age. *Global Biogeochemical Cycles*, *33*, 301–317. https://doi.org/10.1029/2018gb006049

Bernasconi, S. M., Müller, I. A., Bergmann, K. D., Breitenbach, S. F. M., Fernandez, A., Hodell, D. A., et al. (2018). Reducing uncertainties in carbonate clumped isotope analysis through consistent carbonate-based standardization. *Geochemistry, Geophysics, Geosystems*, *19*, 2895–2914. https://doi.org/10.1029/2017gc007385

Bostock, H. C., Opdyke, B. N., & Williams, M. J. M. (2010). Characterising the intermediate depth waters of the Pacific Ocean using δ13C and other geochemical tracers. *Deep Sea Research Part I: Oceanographic Research Papers*, *57*(7), 847–859. https://doi.org/10.1016/j.dsr.2010.04.005

Bradtmiller, L. I., Anderson, R. F., Sachs, J. P., & Fleisher, M. Q. (2010). A deeper respired carbon pool in the glacial equatorial Pacific Ocean. *Earth and Planetary Science Letters*, *299*(3-4), 417–425. https://doi.org/10.1016/j.epsl.2010.09.022

Breitenbach, S. F. M., & Bernasconi, S. M. (2011). Carbon and oxygen isotope analysis of small carbonate samples (20 to 100 μg) with a GasBench II preparation device. *Rapid Communications in Mass Spectrometry*, *25*(13), 1910–1914. https://doi.org/10.1002/rcm.5052

Ceppi, P., Hwang, Y.-T., Liu, X., Frierson, D. M. W., & Hartmann, D. L. (2013). The relationship between the ITCZ and the Southern Hemispheric eddy-driven jet. *Journal of Geophysical Research: Atmospheres*, *118*, 5136–5146. https://doi.org/10.1002/jgrd.50461

Chalk, T. B., Hain, M. P., Foster, G. L., Rohling, E. J., Sexton, P. F., Badger, M. P. S., et al. (2017). Causes of ice age intensification across the Mid-Pleistocene Transition. *Proceedings of the National Academy of Sciences*, *114*(50), 13,114–13,119. https://doi.org/10.1073/pnas.1702143114

Clark, P. U., Archer, D., Pollard, D., Blum, J. D., Rial, J. A., Brovkin, V., et al. (2006). The middle Pleistocene transition: Characteristics, mechanisms, and implications for long-term changes in atmospheric pCO2. *Quaternary Science Reviews*, *25*(23–24), 3150–3184. https://doi.org/10.1016/j.quascirev.2006.07.008

De Baar, H. J. W., Bacon, M. P., Brewer, P. G., & Bruland, K. W. (1985). Rare earth elements in the Pacific and Atlantic oceans. *Geochimica et Cosmochimica Acta*, *49*(9), 1943–1959. https://doi.org/10.1016/0016-7037(85)90089-4

de la Fuente, M., Skinner, L., Calvo, E., Pelejero, C., & Cacho, I. (2015). Increased reservoir ages and poorly ventilated deep waters inferred in the glacial eastern equatorial Pacific. *Nature Communications*, *6*(1). https://doi.org/10.1038/ncomms8420

Denton, G. H., Anderson, R. F., Toggweiler, J. R., Edwards, R. L., Schaefer, J. M., & Putnam, A. E. (2010). The last glacial termination. *Science*, *328*(5986), 1652–1656. https://doi.org/10.1126/science.1184119

Diester-Haass, L., Billups, K., & Lear, C. (2018). Productivity changes across the mid-Pleistocene climate transition. *Earth-Science Reviews*, *179*, 372–391. https://doi.org/10.1016/j.earscirev.2018.02.016

Diz, P., Hernández-Almeida, I., Bernárdez, P., Pérez-Arlucea, M., & Hall, I. R. (2018). Ocean and atmosphere teleconnections modulate east tropical Pacific productivity at late to middle Pleistocene terminations. *Earth and Planetary Science Letters*, *493*, 82–91. https://doi.org/10.1016/j.epsl.2018.04.024

Diz, P., Peñalver-Clavel, I., Hernández-Almeida, I., & Bernasconi, S. M. (2020). Environmental changes in the east equatorial Pacific during the Mid Pleistocene Transition and implications for the last global extinction of benthic foraminifera. *Palaeogeography, Palaeoclimatology, Palaeoecology*, *539*, 109487. https://doi.org/10.1016/j.palaeo.2019.109487

Dubinin, A. V. (2004). Geochemistry of rare earth elements in the ocean. *Lithology and Mineral Resources*, *39*(4), 289–307. https://doi.org/10.1023/B:LIMI.0000033816.14825.a2

Farmer, J. R., Hönisch, B., Haynes, L. L., Kroon, D., Jung, S., Ford, H. L., et al. (2019). Deep Atlantic Ocean carbon storage and the rise of 100,000-year glacial cycles. *Nature Geoscience*, *12*(5), 355–360. https://doi.org/10.1038/s41561-019-0334-6

Farrell, J. W., & Prell, W. L. (1989). Climatic change and CaCO3 preservation: An 800,000 year bathymetric reconstruction from the central equatorial Pacific Ocean. *Paleoceanography*, *4*(4), 447–466. https://doi.org/10.1029/PA004i004p00447

German, C. R., & Elderfield, H. (1990). Application of the Ce anomaly as a paleoredox indicator: The ground rules. *Paleoceanography*, *5*(5), 823–833. https://doi.org/10.1029/PA005i005p00823

Hain, M. P., Sigman, D. M., & Haug, G. H. (2014). The biological pump in the past. In H. D. Holland & K. K. Turekian (Eds.), *Treatise on geochemistry* (Second Edition, pp. 485–517). Elsevier. https://doi.org/10.1016/B978-0-08-095975-7.00618-5

Haley, B. A., Klinkhammer, G. P., & McManus, J. (2004). Rare earth elements in pore waters of marine sediments. *Geochimica et Cosmochimica Acta*, *68*(6), 1265–1279. https://doi.org/10.1016/j.gca.2003.09.012

Hasenfratz, A. P., Jaccard, S. L., Martínez-García, A., Sigman, D. M., Hodell, D. A., Vance, D., et al. (2019). The residence time of Southern Ocean surface waters and the 100,000-year ice age cycle. *Science*, *363*(6431), 1080–1084. https://doi.org/10.1126/science.aat7067

Hönisch, B., Hemming, N. G., Archer, D., Siddall, M., & McManus, J. F. (2009). Atmospheric carbon dioxide concentration across the mid-Pleistocene transition. *Science*, *324*(5934), 1551–1554. https://doi.org/10.1126/science.1171477

Hoogakker, B., Elderfield, H., Oliver, K., & Crowhurst, S. (2010). Benthic foraminiferal oxygen isotope offsets over the last glacial-interglacial cycle. *Paleoceanography*, *25*, PA4229. https://doi.org/10.1029/2009PA001870

Hoogakker, B. A. A., Lu, Z., Umling, N. E., Jones, L., Zhou, X., Rickaby, R. E. M., et al. (2018). Glacial expansion of oxygen-depleted seawater in the eastern tropical Pacific. *Nature*, *562*(7727), 410–413. https://doi.org/10.1038/s41586-018-0589-x

Hughes, P. D., & Gibbard, P. L. (2018). Global glacier dynamics during 100 ka Pleistocene glacial cycles. *Quaternary Research*, *90*(1), 222–243. https://doi.org/10.1017/qua.2018.37

Jaccard, S. L., Hayes, C. T., Martínez-García, A., Hodell, D. A., Anderson, R. F., Sigman, D. M., & Haug, G. H. (2013). Two modes of change in Southern Ocean productivity over the past million years. *Science*, *339*(6126), 1419–1423. https://doi.org/10.1126/science.1227545

Jacobel, A. W., Anderson, R. F., Jaccard, S. L., McManus, J. F., Pavia, F. J., & Winckler, G. (2020). Deep Pacific storage of respired carbon during the last ice age: Perspectives from bottom water oxygen reconstructions. *Quaternary Science Reviews*, *230*, 106065. https://doi.org/10.1016/j.quascirev.2019.106065

Jacobel, A. W., McManus, J. F., Anderson, R. F., & Winckler, G. (2017). Repeated storage of respired carbon in the equatorial Pacific Ocean over the last three glacial cycles. *Nature Communications*, *8*(1), 1727. https://doi.org/10.1038/s41467-017-01938-x

Kemp, A. E. S., Grigorov, I., Pearce, R. B., & Naveira Garabato, A. C. (2010). Migration of the Antarctic polar front through the mid-Pleistocene transition: Evidence and climatic implications. *Quaternary Science Reviews*, *29*(17-18), 1993–2009. https://doi.org/10.1016/j.quascirev.2010.04.027

Kender, S., Ravelo, A. C., Worne, S., Swann, G. E. A., Leng, M. J., Asahi, H., et al. (2018). Closure of the Bering Strait caused mid-Pleistocene transition cooling. *Nature Communications*, *9*(1), 5386. https://doi.org/10.1038/s41467-018-07828-0

Köhler, P., & Bintaja, R. (2008). The carbon cycle during the Mid Pleistocene Transition: The Southern Ocean decoupling hypothesis. *Climate of the Past*, *4*(4), 311–332. https://doi.org/10.5194/cp-4-311-2008

Korff, L., von Dobeneck, T., Frederichs, T., Kasten, S., Kuhn, G., Gersonde, R., & Diekmann, B. (2016). Cyclic magnetite dissolution in Pleistocene sediments of the abyssal Northwest Pacific Ocean: Evidence for glacial oxygen depletion and carbon trapping. *Paleoceanography*, *31*, 600–624. https://doi.org/10.1002/2015PA002882

Larrose, A., Coynel, A., Schäfer, J., Blanc, G., Massé, L., & Maneux, E. (2010). Assessing the current state of the Gironde estuary by mapping priority contaminant distribution and risk potential in surface sediment. *Applied Geochemistry*, *25*(12), 1912–1923. https://doi.org/10.1016/j.apgeochem.2010.10.007

Le, J., & Shackleton, N. J. (1992). Carbonate dissolution fluctuations in the Western equatorial Pacific during the late quaternary. *Paleoceanography*, *7*(1), 21–42. https://doi.org/10.1029/91pa02854

Lear, C. H., Billups, K., Rickaby, R. E. M., Diester-Haass, L., Mawbey, E. M., & Sosdian, S. M. (2016). Breathing more deeply: Deep ocean carbon storage during the mid-Pleistocene climate transition. *Geology*, *44*(12), 1035–1038. https://doi.org/10.1130/G38636.1

Licari, L., Schumacher, S., Wenzhöfer, F., Zabel, M., & Mackensen, A. (2003). Communities and microhabitats of living benthic foraminifera from the tropical East Atlantic: Impact of different productivity regimes. *Journal of Foraminiferal Research*, *33*(1), 10–31. https://doi.org/10.2113/0330010

Lisiecki, L. E. (2010a). A benthic δ13C-based proxy for atmospheric pCO2 over the last 1.5 Myr. *Geophysical Research Letters*, *37*, L21708. https://doi.org/10.1029/2010GL045109

Lisiecki, L. E. (2010b). A simple mixing explanation for the late Pleistocene changes in the Pacific-South Atlantic benthic d13C gradient. *Climate of the Past*, *6*(3), 305–314. https://doi.org/10.5194/cp-6-305-2010

Lisiecki, L. E., & Raymo, M. E. (2005). A Pliocene-Pleistocene stack of 57 globally distributed benthic δ18O records. *Paleoceanography*, *20*, PA1003. https://doi.org/10.1029/2004PA001071

Liu, Z., & Herbert, T. D. (2004). High-latitude influence on the eastern equatorial Pacific climate in the early Pleistocene epoch. *Nature*, *427*(6976), 720–723. https://doi.org/10.1038/nature02338

López-Otálvaro, G. E., Flores, J. A., Sierro, F. J., & Cacho, I. (2008). Variations in coccolithophorid production in the eastern equatorial Pacific at ODP site 1240 over the last seven glacial–interglacial cycles. *Marine Micropaleontology*, *69*(1), 52–69. https://doi.org/10.1016/j.marmicro.2007.11.009

López-Otálvaro, G. E., Flores, J. A., Sierro, F. J., Lalicata, J., Lea, D. W., & Mix, A. (2019). Deciphering latitudinal shifts in coccolith accumulation in the eastern tropical Pacific Ocean through the Pleistocene. *Marine Micropaleontology*, *152*, 101739. https://doi.org/10.1016/j.marmicro.2019.03.011

Loveley, M. R., Marcantonio, F., Wisler, M. M., Hertzberg, J. E., Schmidt, M. W., & Lyle, M. (2017). Millennial-scale iron fertilization of the eastern equatorial Pacific over the past 100,000 years. *Nature Geoscience*, *10*(10), 760–764. https://doi.org/10.1038/ngeo3024

Ma, Z., Ravelo, A. C., Liu, Z., Zhou, L., & Paytan, A. (2015). Export production fluctuations in the eastern equatorial Pacific during the Pliocene-Pleistocene: Reconstruction using barite accumulation rates. *Paleoceanography*, *30*, 1455–1469. https://doi.org/10.1002/2015pa002860

Mackensen, A., & Schmiedl, G. (2019). Stable carbon isotopes in paleoceanography: Atmosphere, oceans, and sediments. *Earth-Science Reviews*, *197*, 102893. https://doi.org/10.1016/j.earscirev.2019.102893

Martinez-Boti, M. A., Marino, G., Foster, G. L., Ziveri, P., Henehan, M. J., Rae, J. W. B., et al. (2015). Boron isotope evidence for oceanic carbon dioxide leakage during the last deglaciation. *Nature*, *518*(7538), 219–222. https://doi.org/10.1038/nature14155

Martínez-Méndez, G., Hebbeln, D., Mohtadi, M., Lamy, F., De Pol-Holz, R., Reyes-Macaya, D., & Freudenthal, T. (2013). Changes in the advection of Antarctic intermediate water to the northern Chilean coast during the last 970 kyr. *Paleoceanography*, *28*, 607–618. https://doi.org/10.1002/palo.20047

McClymont, E. L., Sosdian, S. M., Rosell-Melé, A., & Rosenthal, Y. (2013). Pleistocene Sea-surface temperature evolution: Early cooling, delayed glacial intensification, and implications for the mid-Pleistocene climate transition. *Earth-Science Reviews*, *123*, 173–193. https://doi.org/10.1016/j.earscirev.2013.04.006

Menviel, L., Spence, P., Yu, J., Chamberlain, M. A., Matear, R. J., Meissner, K. J., & England, M. H. (2018). Southern hemisphere westerlies as a driver of the early deglacial atmospheric CO2 rise. *Nature Communications*, *9*(1), 2503. https://doi.org/10.1038/s41467-018-04876-4

Mills, R. A., Taylor, S. L., Pälike, H., & Thomson, J. (2010). Hydrothermal sediments record changes in deep water oxygen content in the SE Pacific. *Paleoceanography*, *25*, PA4226. https://doi.org/10.1029/2010PA001959

Mix, A. C., Tiedemann, R., Blum, P. (2003). Site 1242. *Proceedings of the Ocean Drilling Program, Initial Reports Volume 202*. Retrieved from doi:https://doi.org/10.2973/odp.proc.ir.202.113.2003

Morford, J. L., & Emerson, S. (1999). The geochemistry of redox sensitive trace metals in sediments. *Geochimica et Cosmochimica Acta*, *63*(11-12), 1735–1750. https://doi.org/10.1016/S0016-7037(99)00126-X

Murray, R. W., Knowlton, C., Leinen, M., Mix, A. C., & Polsky, C. H. (2000). Export production and carbonate dissolution in the central equatorial Pacific Ocean over the past 1 Myr. *Paleoceanography*, *15*(6), 570–592. https://doi.org/10.1029/1999pa000457

Pattan, J. N., Parthiban, G., Garg, A., & Moraes, N. R. C. (2017). Intense reducing conditions during the last deglaciation and Heinrich events (H1, H2, H3) in sediments from the oxygen minimum zone off Goa, eastern Arabian Sea. *Marine and Petroleum Geology*, *84*, 243–256. https://doi.org/10.1016/j.marpetgeo.2017.03.034

Pena, L. D., & Goldstein, S. L. (2014). Thermohaline circulation crisis and impacts during the mid-Pleistocene transition. *Science*, *345*(6194), 318–322. https://doi.org/10.1126/science.1249770

Peterson, L. C., & Prell, W. L. (1985). Carbonate dissolution in recent sediments of the eastern equatorial Indian Ocean: Preservation patterns and carbonate loss above the lysocline. *Marine Geology*, *64*(3-4), 259–290. https://doi.org/10.1016/0025-3227(85)90108-2

Rae, J. W. B., Burke, A., Robinson, L. F., Adkins, J. F., Chen, T., Cole, C., et al. (2018). CO2 storage and release in the deep Southern Ocean on millennial to centennial timescales. *Nature*, *562*(7728), 569–573. https://doi.org/10.1038/s41586-018-0614-0

Railsback, L. B., Gibbard, P. L., Head, M. J., Voarintsoa, N. R. G., & Toucanne, S. (2015). An optimized scheme of lettered marine isotope substages for the last 1.0 million years, and the climatostratigraphic nature of isotope stages and substages. *Quaternary Science Reviews*, *111*, 94–106. https://doi.org/10.1016/j.quascirev.2015.01.012

Raymo, M. E., & Nisancioglu, K. H. (2003). The 41 kyr world: Milankovitch's other unsolved mystery. *Paleoceanography*, *18*(1). https://doi.org/10.1029/2002pa000791

Rudnick, R. L., & Gao, S. (2014). 4.1 - composition of the continental crust A2 - Holland, Heinrich D. In K. K. Turekian (Ed.), *Treatise on Geochemistry*, (Second ed.pp. 1–51). Oxford: Elsevier. https://doi.org/10.1016/B978-0-08-095975-7.00301-6

Schindlbeck, J. C., Kutterolf, S., Freundt, A., Alvarado, G. E., Wang, K. L., Straub, S. M., et al. (2016). Late Cenozoic tephrostratigraphy offshore the southern central American volcanic arc: 1. Tephra ages and provenance. *Geochemistry, Geophysics, Geosystems*, *17*, 4641–4668. https://doi.org/10.1002/2016gc006503

Schmittner, A., Bostock, H. C., Cartapanis, O., Curry, W. B., Filipsson, H. L., Galbraith, E. D., et al. (2017). Calibration of the carbon isotope composition (δ13C) of benthic foraminifera. *Paleoceanography*, *32*, 512–530. https://doi.org/10.1002/2016pa003072

Schoepfer, S. D., Shen, J., Wei, H., Tyson, R. V., Ingall, E., & Algeo, T. J. (2015). Total organic carbon, organic phosphorus, and biogenic barium fluxes as proxies for paleomarine productivity. *Earth-Science Reviews*, *149*, 23–52. https://doi.org/10.1016/j.earscirev.2014.08.017

Scudder, R. P., Murray, R. W., Schindlbeck, J. C., Kutterolf, S., Hauff, F., Underwood, M. B., et al. (2016). Geochemical approaches to the quantification of dispersed volcanic ash in marine sediment. *Progress in Earth and Planetary Science*, *3*(1), 1. https://doi.org/10.1186/s40645-015-0077-y

Sexton, P. F., & Barker, S. (2012). Onset of 'Pacific-style' deep-sea sedimentary carbonate cycles at the mid-Pleistocene transition. *Earth and Planetary Science Letters*, *321-322*, 81–94. https://doi.org/10.1016/j.epsl.2011.12.043

Sigman, D. M., Hain, M. P., & Haug, G. H. (2010). The polar ocean and glacial cycles in atmospheric CO2 concentration. *Nature*, *466*(7302), 47–55. https://doi.org/10.1038/nature09149

Spero, H. J., & Lea, D. W. (2002). The cause of carbon isotope minimum events on glacial terminations. *Science*, *296*(5567), 522–525. https://doi.org/10.1126/science.1069401

Stramma, L., Johnson, G. C., Firing, E., & Schmidtko, S. (2010). Eastern Pacific oxygen minimum zones: Supply paths and multidecadal changes. *Journal of Geophysical Research*, *115*, C09011. https://doi.org/10.1029/2009jc005976

Suzuki, T., Ishii, M., Aoyama, M., Christian, J. R., Enyo, K., Kawano, T., . . . Sabine, C. L. (2013). PACIFICA Data Synthesis Project. ORNL/CDIAC-159, NDP-092. Carbon Dioxide Information Analysis Center, Oak Ridge. Retrieved from Ridge, Tennessee:

Talley, L. D. (2013). Closure of the global overturning circulation through the Indian, Pacific, and southern oceans: Schematics and transports. *Oceanography*, *26*(1), 80–97. https://doi.org/10.5670/oceanog.2013.07

Thomas, E., Turekian, K. K., & Wei, K. Y. (2000). Productivity control of fine particle transport to equatorial Pacific sediment. *Global Biogeochemical Cycles*, *14*(3), 945–955. https://doi.org/10.1029/1998gb001102

Thunell, R. C., Keir, R. S., & Honjo, S. (1981). Calcite dissolution: An in situ study in the Panama Basin. *Science*, *212*(4495), 659–661. https://doi.org/10.1126/science.212.4495.659

Tostevin, R., Shields, G. A., Tarbuck, G. M., He, T., Clarkson, M. O., & Wood, R. A. (2016). Effective use of cerium anomalies as a redox proxy in carbonate-dominated marine settings. *Chemical Geology*, *438*, 146–162. https://doi.org/10.1016/j.chemgeo.2016.06.027

Tribovillard, N., Algeo, T. J., Lyons, T., & Riboulleau, A. (2006). Trace metals as paleoredox and paleoproductivity proxies: An update. *Chemical Geology*, *232*(1–2), 12–32. https://doi.org/10.1016/j.chemgeo.2006.02.012

Tziperman, E., & Gildor, H. (2003). On the mid-Pleistocene transition to 100-kyr glacial cycles and the asymmetry between glaciation and deglaciation times. *Paleoceanography*, *18*(1), 1-1–1-8. https://doi.org/10.1029/2001pa000627

Umling, N. E., & Thunell, R. C. (2017). Synchronous deglacial thermocline and deep-water ventilation in the eastern equatorial Pacific. *Nature Communications*, *8*(1), 14,203. https://doi.org/10.1038/ncomms14203

Umling, N. E., Thunell, R. C., & Bizimis, M. (2018). Deepwater expansion and enhanced Remineralization in the eastern equatorial Pacific during the last glacial maximum. *Paleoceanography and Paleoclimatology*, *33*, 563–578. https://doi.org/10.1029/2017PA003221

Zheng, Y., Anderson, R. F., van Geen, A., & Fleisher, M. Q. (2002). Preservation of particulate non-lithogenic uranium in marine sediments. *Geochimica et Cosmochimica Acta*, *66*(17), 3085–3092. https://doi.org/10.1016/S0016-7037(01)00632-9

References From the Supporting Information

Knudson, K. P., & Ravelo, A. C. (2015). North Pacific intermediate water circulation enhanced by the closure of the Bering Strait. *Paleoceanography*, *30*, 1287–1304. https://doi.org/10.1002/2015PA002840

Lalicata, J. J., & Lea, D. W. (2011). Pleistocene carbonate dissolution fluctuations in the eastern equatorial Pacific on glacial timescales: Evidence from ODP hole 1241. *Marine Micropaleontology*, *79*(1–2), 41–51. https://doi.org/10.1016/j.marmicro.2011.01.002

Rippert, N., Max, L., Mackensen, A., Cacho, I., Povea, P., & Tiedemann, R. (2017). Alternating influence of northern versus southern-sourced water masses on the equatorial Pacific subthermocline during the past 240 ka. *Paleoceanography*, *32*, 1256–1274. https://doi.org/10.1002/2017pa003133